ISSN 1062-8738, Bulletin of the Russian Academy of Sciences: Physics, 2024, Vol. 88, Suppl. 3, pp. S423–S427. © Pleiades Publishing, Ltd., 2024.

Results of Lidar Observations of Long-Range Transport of Dust Aerosol from the Gobi and Taklamakan Deserts to the Troposphere of Vladivostok

V. V. Lisitsa[a], K. A. Shmirko[a, *], A. N. Pavlov[a], and O. G. Konstantinov[b]

[a] *Institute of Automation and Control Processes, Far Eastern Branch, Russian Academy of Sciences, Vladivostok, 690041 Russia*

[b] *Il'ichev Pacific Oceanological Institute, Far Eastern Branch, Russian Academy of Sciences, Vladivostok, 690041 Russia*

**e-mail: kshmirko@vk.com*

Received October 31, 2024; revised November 15, 2024; accepted November 28, 2024

Abstract—The results of lidar measurements of the vertical distribution of optical properties of dust aerosol from the Gobi and Taklamakan deserts in the free troposphere over Vladivostok are presented. A Mi-Raman lidar with a cross-polarization channel was used as an instrument, allowing for the retrieval of vertical profiles of a set of ($3\beta + 2\varepsilon + \delta$) three backscattering coefficients (355, 532, 1064 nm), two extinction coefficients, and one depolarization coefficient at a wavelength of 532 nm. A high depolarization coefficient value (δ = 0.13–0.15), characteristic of submicrometer-sized dust aerosol particles, was observed in the altitude range of 3.00–4.25 km for the dust aerosol from the Gobi Desert. For the aerosol recorded from the Taklamakan Desert, this value was $\delta = 0.14$ in the altitude range of 5–10 km. To obtain information on the spatial distribution of microphysical characteristics, an inversion procedure ($3\beta + 2\varepsilon + \delta$) based on the model of randomly oriented spheroids was used. The complex refractive index within the dust layer had values typical for dust particles, with m_r = 1.48–1.56 and m_i = 0.001 for the aerosol from the Gobi Desert, and m_r = 1.51–1.61 for the aerosol from the Taklamakan Desert.

Keywords: dust aerosol, lidar sounding, depolarisation ratio

DOI: 10.1134/S1062873824709954

INTRODUCTION

Interest in studying atmospheric aerosol and its variability is driven by uncertainties in assessments of climate and ecological impacts. Dust aerosol, particularly from arid regions covering about 30% of the Earth's surface, significantly contributes to this uncertainty, with soil minerals accounting for up to 75% of the aerosol load [1, 2].

East Asia is home to two main sources of dust aerosol: the Taklamakan Desert in China and the Gobi Desert. Dust storms in these areas exhibit pronounced seasonal patterns, with peak activity in spring. Approximately 30% of the dust aerosol lifted into the atmosphere returns to its source, 20% remains in Eurasia, and 50% is transported eastward [3].

The transport characteristics of aerosol vary in the Tarim Basin, only fine particles can reach heights of 5 km and be carried by jet streams, while aerosol from the Gobi is most actively spread to eastern regions, including Japan and western North America, in the lower layers of the atmosphere [4, 5]. Two jet streams over the Gobi create conditions conducive to efficient transport at altitudes of 2–4 km, and the mixing of dust aerosol with anthropogenic pollutants in industrial regions of China alters its microphysical and optical properties [6].

EQUIPMENT AND METHODS

A multi-wavelength Mi-Raman lidar based on an Nd:YAG laser, equipped with a channel for measuring the depolarization coefficient at a wavelength of 532 nm, was used as the primary instrument for investigating the vertical distribution of optical properties of atmospheric aerosol. Modern Raman three-wavelength lidars can obtain vertical profiles of three backscattering coefficients, two extinction coefficients, and the depolarization coefficient at one of the probing wavelengths ($3\beta + 2\varepsilon + \delta$).

The lidar design involves measuring three backscattering coefficients (at wavelengths of 355, 532, and 1064 nm), two extinction coefficients (at 355 and 532 nm), and the depolarization ratio at a wavelength of 532 nm.

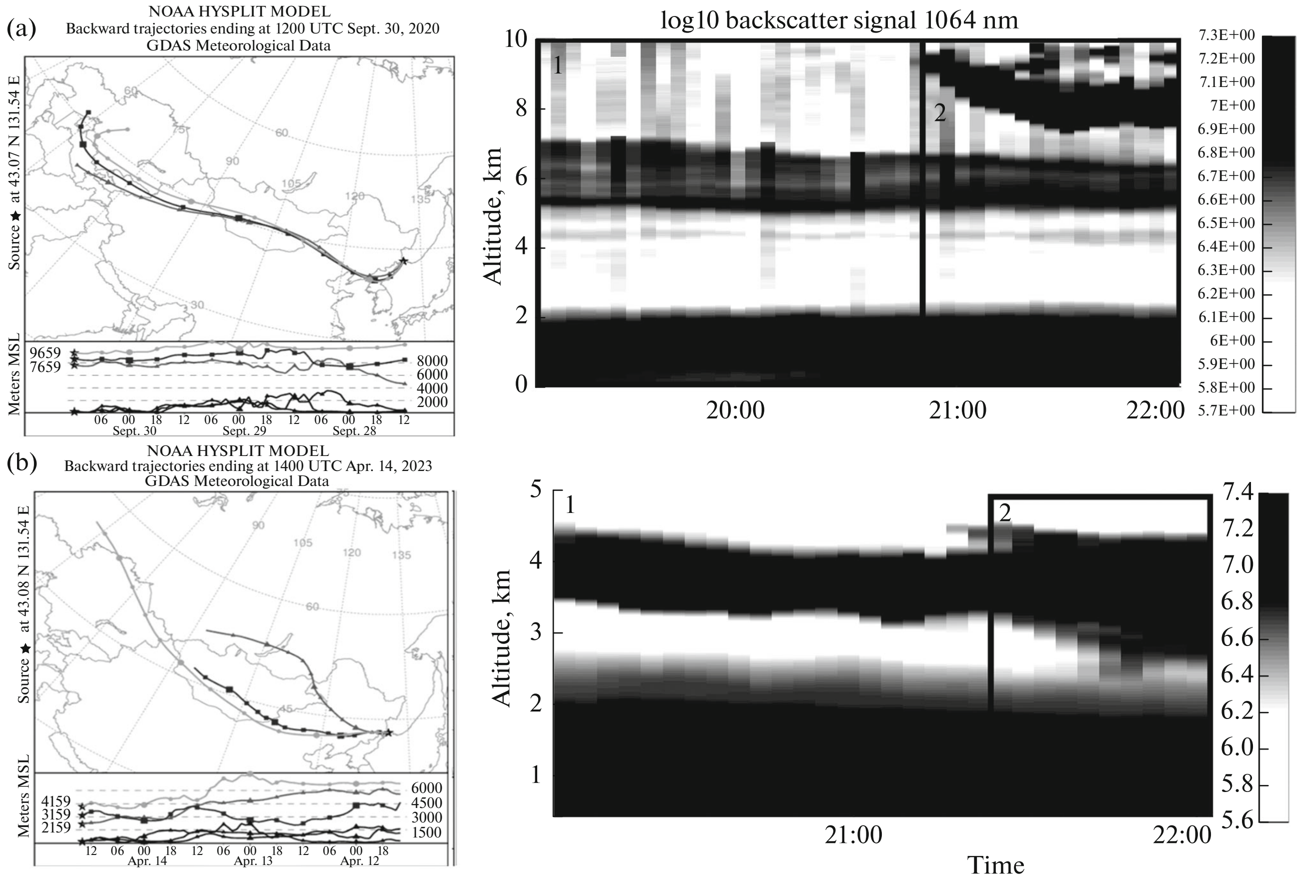

Fig 1. Time history of backscatter signal at 1064 nm wavelength and back trajectory analysis for desert aerosol: (a) Taklamakan, (b) Gobi.

One of the important optical parameters reflecting the degree of non-sphericity of aerosol particles is the linear depolarization ratio of aerosol particles. Typically, this value is used in lidar probing to determine aerosol types and is calculated using the equation:

$$\delta_p = \frac{R\delta_v(\delta_m + 1) - \delta_m(\delta_v + 1)}{R\delta_v(\delta_m + 1) - (\delta_v + 1)}. \quad (1)$$

Where R is the scattering ratio, δ_v is the degree of volume linear depolarization, and δ_m is the depolarization ratio. R is defined as the ratio of the total backscattering coefficient to the molecular backscattering coefficient; $\delta_m = 0.004$; δ_v is the volume depolarization coefficient, determined as the ratio of the cross-polarized signal to the backscattered signal, multiplied by a calibration constant. The calibration constant was calculated using the method described in [7].

The microphysical characteristics of aerosol particles were determined using an inversion algorithm based on light scattering modeling with spheres for the case of $\delta_p \leq 10\%$ and a set of randomly oriented spheroids for the case of $\delta_p \geq 10\%$ [8].

VERTICAL DISTRIBUTION OF OPTICAL AND MICROPHYSICAL CHARACTERISTICS OF AEROSOL PARTICLES

In Fig. 1a, the temporal waveform of the backscattered signal and the transport trajectories of air masses are presented of dust transport recorded during the autumn period on September 30, 2020. Figure 1b shows similar characteristics for April 14, 2023. The calculation of back trajectories was performed using the HYSPLIT model.

In Fig. 1a, there was only one aerosol layer with a vertical extent of 3.00 km, located centrally at an altitude of 6.5 km. Starting at 21:00 local time, a more intense layer at an altitude of 9.00 km was added. Our further studies of the optical characteristics will focus on this section, marked with the letter 2 in Fig. 1a. The results of the back trajectory analysis indicate that the air masses passed near the northern boundary of the Taklamakan Desert and over the southern regions of Mongolia.

As shown in Fig. 1b, the dust layer with a vertical extent of 1250 m was situated at the lower level of the free troposphere, close to the planetary boundary layer

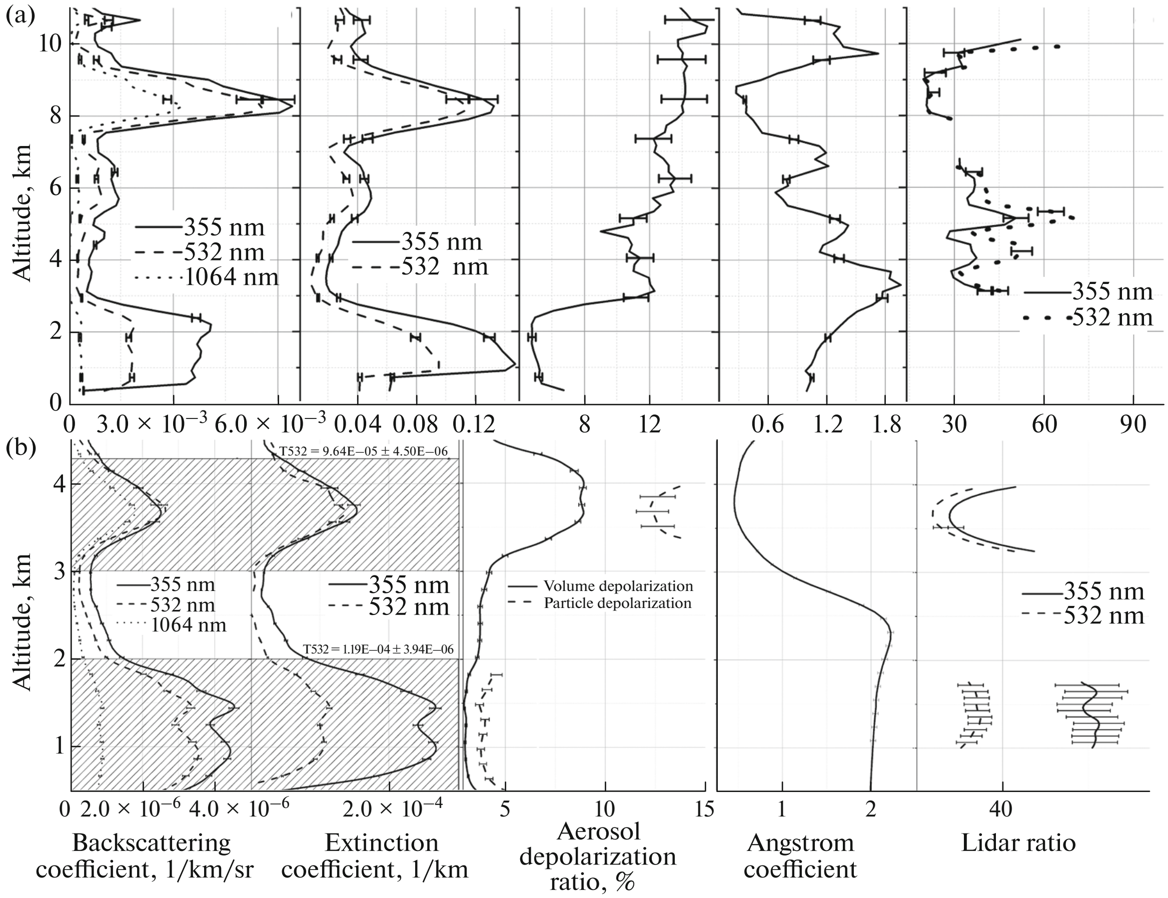

Fig. 2. Vertical profiles of optical characteristics: backscattering and attenuation coefficients, aerosol depolarization ratio, angstrom coefficient and lidar ratio for desert aerosol: (a) Taklamakan, (b) Gobi.

(PBL), which did not exceed 2000 meters in height during this period.

The high degree of depolarization within the dust layer, $\delta_p = 0.14$ (Fig. 2a) and $\delta_p = 0.13$ (Fig. 2b), characteristic of the submicrometer fraction of dust aerosol [9], indicates that the aerosol particles are predominantly irregular in shape [10].

In Fig. 2b, two layers of light scattering are clearly visible in the vertical profile. The first layer is in the height range of 500–2000 m, while the second is in the range of 3000–4250 m. This indicates exchange processes between the layers, including the dry deposition of dust aerosol. The Angstrom exponent remains constant throughout the PBL, with a value of $\alpha_{355/532} = 2$; however, within the dust layer, its value varies significantly, ranging from $\alpha_{355/532} = 2$ at the boundaries to 0.4 in the middle. Such variation in the exponent suggests a noticeable increase in the size of dust particles within the layer.

In Fig. 2a, a two-layer structure of the dust cloud is noted, where the minimum values of the Angstrom exponent are recorded at altitudes of 6.00 and 8.50 km, measuring 0.7 and 0.3, respectively. Assuming a constant composition of the dust aerosol at all heights, this indicates local maxima in dust particle sizes at these altitudes and an increase in their sizes in the upper layer.

To assess the microphysical characteristics of aerosol particles, we used an inversion algorithm [8] employing a model based on Mie theory within the PBL, and a model for the scattering properties of randomly oriented spheroids within the dust layer. The boundaries for the permissible values for the minimum and maximum particle radius sizes were set at 0.03 and 10 μm, respectively. For the real part of the refractive index, values were allowed in the range of $m_r = 1.35$ to 1.6, while for the imaginary part, $m_i = 0$–0.02. The refractive index was spectrally independent and independent of particle size.

The available studies present methods for assessing the concentration of fine particulate matter in the atmosphere [11]. In Fig. 3b, the vertical profile of volumetric concentration is presented, showing an approximate equality of aerosol particle volumetric concentrations in the PBL and at the level of the dust layer. The effective radius throughout the PBL is con-

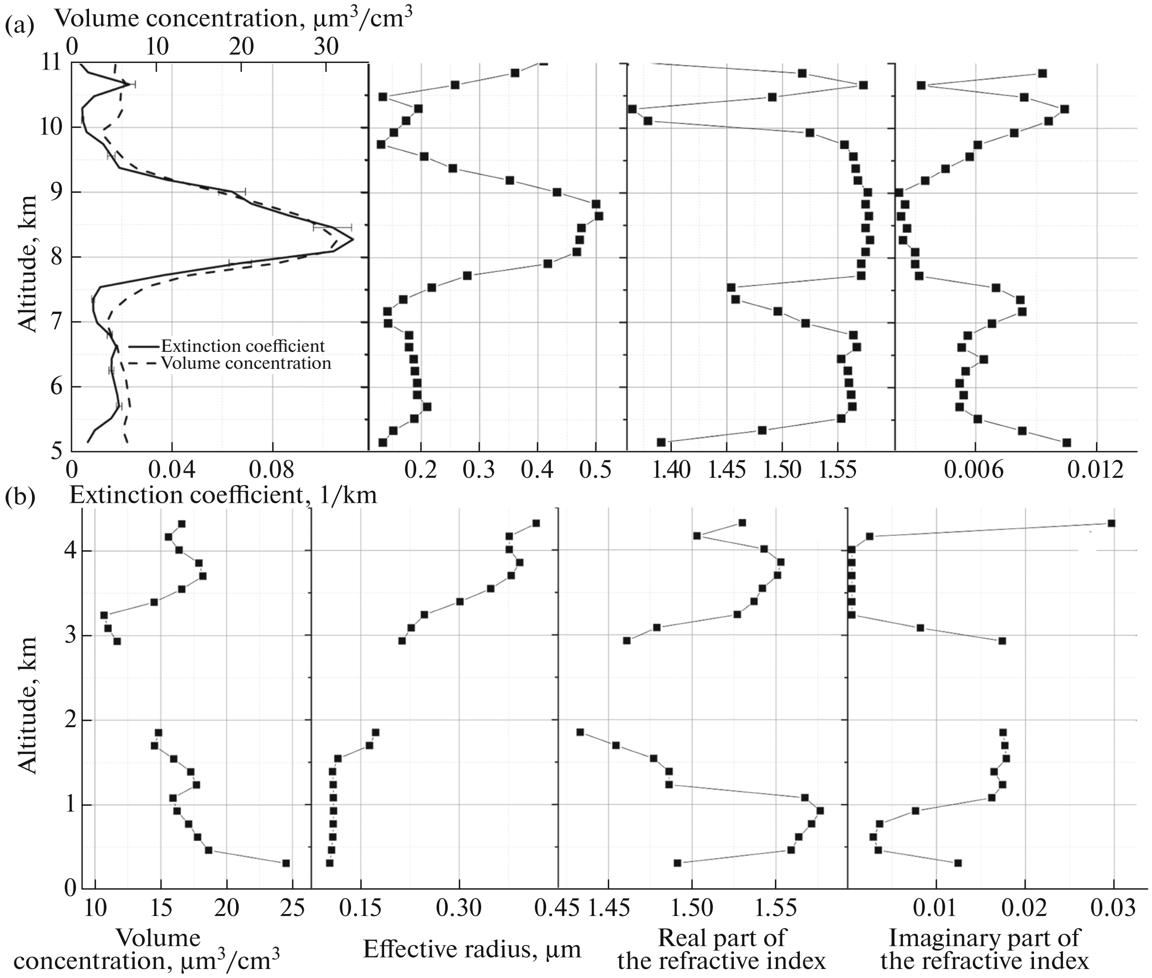

Fig. 3. Vertical profiles of microphysical characteristics of aerosol particles: volume concentration, effective radius, real and imaginary part of refractive index for desert aerosol: (a) Taklamakan, (b) Gobi.

stant at $r_{\mathrm{eff}} = 0.11$ μm, while within the dust layer, it monotonically increases from 0.2 to 0.4 μm with height. For the dust layer in the range of 3000–4250 m, the real part of the refractive index $m_r = 1.55$ is in good agreement with literature values for dust particles [12]. Within the PBL, its value varies from 1.45 to 1.56 as height decreases

Figure 3a shows the height profile of aerosol particle volumetric concentration along with the extinction coefficient profile ε_{532}. The maximum volumetric concentration, reaching 30 μm^3/cm^3, is recorded in the upper aerosol layer at an altitude of 8.50 km, which is more than five times greater than the concentration in the lower layer.

This maximum volumetric concentration corresponds to the maximum effective radius of aerosol particles, the vertical distribution of which is shown in Fig. 3b. The significant difference in effective radius values between the aerosol layers—0.38 μm in the upper layer and 0.16 μm in the lower layer—can be explained by hygroscopic growth of particles in the upper layer and nucleation processes. This is also supported by the low lidar ratios at an altitude of 8.00 km, discussed earlier. The real part of the refractive index in the aerosol layers varies from 1.55 ± 0.05 to 1.57 ± 0.05.

CONCLUSIONS

In this study, we presented only two episodes of dust aerosol registration: from the Gobi and Taklamakan deserts, and based on these, we demonstrated regional patterns of vertical distribution of optical and microphysical characteristics in the atmosphere of Vladivostok. These patterns include the height corridor for dust plume transport from the Gobi Desert, which ranges from 3 to 6 km, and from the Taklamakan Desert, which occurs near the tropopause at altitudes of 8–13 km. Another distinguishing feature of the Asian dust aerosol supplied to the atmosphere of southern Primorsky krai and adjacent marine areas is the size of the dust particles, which belong to the submicrometer fraction of atmospheric aerosol.

In April–May 2009, measurements of atmospheric aerosol properties were conducted in Primorsky krai using sun photometry, lidar profiling, and sampling aboard the training vessel "Nadezhda." It was found that in spring, the region's atmosphere is influenced by multiple sources of aerosol, including dust emissions from arid areas. The turbidity of the atmosphere over the Sea of Japan was significantly higher than in other temperate oceanic zones (approximately 2 times higher) and even compared to the trade wind zone of the Atlantic. However, a fine aerosol fraction predominates over the Sea of Japan, in contrast to the coarse fraction in the Atlantic [4].

FUNDING

The results of the study of aerosol deposition processes were obtained with the support of the Russian Science Foundation (grant no. 23-77-00004). The results regarding the modification of aerosol characteristics during long-range transport were funded by the state budget theme no. 01021353011.

CONFLICT OF INTEREST

The authors of this work declare that they have no conflicts of interest.

REFERENCES

1. Bauer, E. and Ganopolski, A., *Clim. Past*, 2014, vol. 10, no. 4, p. 149.
2. Gubanova, D.P., Vinogradova, A.A., and Sadovskaya, N.V., *Bull. Russ. Acad. Sci.: Phys.*, 2023, vol. 87, no. 10, p. 1411.
3. Zhang, X.Y., Arimoto, R., and An, Z.S., *J. Geophys. Res.: Atmos.*, 1997, vol. 102, p. 28041.
4. Sakerin, S.M., Pavlov, A.N., Bukin, O.A., Kabanov, D.M., Kornienko, G.I., Polkin, V.V., Stolyarchuk, S.Yu., Turchinovich, Yu.S., Shmirko, K.A., and Mayor, A.Yu., *Atmos. Oceanic Opt.*, 2010, vol. 20, no. 4, p. 306.
5. Liu, L., Guo, J., Gong, H., Li, Z., Chen, W., Wu, R., Wang, L., Xu, H., Li, J., Chen, D., and Zhai, P., *Geophys. Res. Lett.*, 2019, vol. 46, p. 9064.
6. Yu, X., Cheng, T., Chen, J., and Liu, Y., *Atmos. Environ.*, 2006, vol. 40, no. 30, p. 5787.
7. Freudenthaler, V., Esselborn, M., Wiegner, M., Heese, B., Tesche, M., Ansmann, A., Müller, D., Althausen, D., Wirth, M., Fix, A., Ehret, G., Knippertz, P., Toledano, C., Gasteiger, J., Garhammer, M., and Seefeldner, M., *Tellus B*, 2009, vol. 61, p. 165.
8. Veselovskii, I., Dubovik, O., Kolgotin, A., Lapyonok, T., Di Girolamo, P., Summa, D., Whiteman, D.N., Mishchenko, M., and Tanré, D., *J. Geophys. Res.: Atmos.*, 2010, vol. 115, no. D21, p. D21203.
9. Mamouri, R.-E. and Ansmann, A., *Atmos. Meas. Tech.*, 2017, vol. 10, no. 9, p. 3403.
10. Shishko, V.A., Konoshonkin, A.V., Timofeev, D.N., et al., *Bull. Russ. Acad. Sci.: Phys.*, 2022, vol. 86, no. 1 (suppl.), p. S207.
11. Fang, Zh., Yang, H., Zhao, M., Cao, Y., Li, Ch., Xing, K., Deng, X., Xie, Ch., and Liu, D., *J. Appl. Spectrosc.*, 2021, vol. 88, no. 4, p. 616.
12. Jianrong, B., Jinsen, S.H., Yongkun, X., and Yuzhi, L., *J. Meteorol. Soc. Jpn.*, 2014, vol. 92A, p. 33.